Full paper / Mémoire

Extraction and complexation of lanthanide ions by dihomooxacalix[4]arene and calix[4]arene tetraketone derivatives: An experimental and molecular dynamics investigation

Extraction et complexation d'ions lanthanide par des dérivés tétracétone du dihomooxacalix[4]arène et du calix[4]arène : étude expérimentale et dynamique moléculaire

Joel D. Fonseca [a], Paula M. Marcos [a, b, *], José R. Ascenso [c], Sylvia Michel [d], Véronique Hubscher-Bruder [d, **], Rachel Schurhammer [e]

[a] Centro de Química Estrutural, Faculdade de Ciências da Universidade de Lisboa, Edifício C8, 1749-016 Lisboa, Portugal
[b] Faculdade de Farmácia da Universidade de Lisboa, Av. Prof. Gama Pinto, 1649-003 Lisboa, Portugal
[c] Centro de Química Estrutural, Instituto Superior Técnico, Av. Rovisco Pais, 1049-001 Lisboa, Portugal
[d] Université de Strasbourg, CNRS, IPHC UMR 7178, 67000 Strasbourg, France
[e] Université de Strasbourg, Laboratoire de modélisation et simulations moléculaires, UMR 7140, 67000 Strasbourg, France

ARTICLE INFO

ABSTRACT

Lanthanide cation binding by tetraketone derivatives of p-$tert$-butyldihomooxacalix[4]arene (methyl **1a**, $tert$-butyl **1b**, adamantyl **1c** and phenyl **1d**) and of p-$tert$-butylcalix[4]arene (methyl **2a**, adamantyl **2c** and phenyl **2d**), in the cone conformation, was investigated. These properties were assessed by extraction experiments of the metal picrates from water to dichloromethane and by stability constant measurements in acetonitrile by UV-vis absorption spectrophotometry. Proton NMR titrations with La^{3+}, Eu^{3+} and Yb^{3+} cations were also performed to obtain information on the binding sites. Molecular dynamics (MD) simulations and potential of mean force (PMF) free energy calculations were carried out for ligands **1d** and **2d** in pure solvents and at a CH_2Cl_2/water interface to add further information on the complexation and extraction processes. Comparison between dihomooxacalix[4]arene and calix[4]arene ketone derivatives showed that the former are better extractants, displaying the highest percentages of extraction for Gd^{3+} and Yb^{3+} cations. Concerning complexation, all ligands studied presented high affinities for the lanthanide ions. Ligands **1b** and **1d** showed preference for the light La^{3+}, while **2d** displayed the strongest affinity for the heavy and smaller Yb^{3+}. These results were also corroborated by MD simulations, which revealed specificities of ligands **1d** and **2d** in the binding of lanthanide cations.

© 2019 Académie des sciences. Published by Elsevier Masson SAS. All rights reserved.

* Corresponding author. Centro de Química Estrutural, Faculdade de Ciências da Universidade de Lisboa, Edifício C8, 1749-016 Lisboa, Portugal.
** Corresponding author.
E-mail address: pmmarcos@fc.ul.pt (P.M. Marcos).

R É S U M É

Mots-clés:
Calix[4]arène cétones
Dihomooxacalix[4]arène cétones
Interaction avec des cations lanthanide
Spectrophotométrie UV–visible
Spectrométrie RMN du proton
Simulations DM

L'interaction entre des cations lanthanide et des dérivés tétracétone du *p-tert*-butyldi-/homooxacalix[4]arène (méthyl **1a**, *tert*-butyl **1b**, adamantyl **1c** et phényl **1d**) et du *p-tert*-butylcalix[4]arène (méthyl **2a**, adamantyl **2c** et phényl **2d**), en conformation cône, a été étudiée. Ces propriétés ont été évaluées par des expériences d'extraction de picrates métalliques de l'eau vers le dichlorométhane et par la détermination des constantes de stabilité dans l'acétonitrile par spectrophotométrie d'absorption dans l'UV–visible. Des titrages RMN du proton avec les cations La^{3+}, Eu^{3+} et Yb^{3+} ont également été effectués afin d'obtenir des informations sur les sites de liaison. Des simulations en dynamique moléculaire (DM) et des calculs d'énergie libre du potentiel de force moyenne (PMF) ont été réalisés avec les ligands **1d** et **2d** dans les solvants purs et à l'interface CH$_2$Cl$_2$/eau afin d'apporter des informations complémentaires sur les processus de complexation et d'extraction. La comparaison entre les dérivés cétone du dihomooxacalix[4]arène et du calix[4]arène a montré que les premiers possèdent un meilleur pouvoir extractant, avec les pourcentages d'extraction les plus élevés pour les cations Gd^{3+} et Yb^{3+}. Concernant la complexation, tous les ligands étudiés présentent des affinités élevées pour les ions lanthanide. Les ligands **1b** et **1d** montrent une préférence pour La^{3+}, cation léger, alors que **2d** présente la plus forte affinité pour Yb^{3+}, cation lourd et moins volumineux. Ces résultats ont également été confirmés par des simulations en DM, qui ont révélé les spécificités des ligands **1d** et **2d** lors de leur interaction avec les cations lanthanide.

1. Introduction

Since the 1960s, lanthanides have gained a growing importance because of their broad variety of technological applications and use in the industry. These elements are incorporated in materials for catalysis, optics, magnets and electronics [1], in metallurgy and in medicine, where they are used as contrast agents for magnetic resonance imaging, as luminescent probes for diagnostics and as optical imaging of cells [2,3]. They are also connected to radioactive wastes because they are present, together with actinides, in acidic effluents from where they need to be extracted.

Macrocyclic ligands have been extensively developed concerning lanthanide coordination chemistry, mainly those possessing a high number of donor atoms, as lanthanide ions require a coordination number of eight or nine. Among them, calixarenes and their derivatives have been largely used in metal cation binding in the last three decades. In particular, the capacity of carbonyl-containing substituents on the lower rim of calixarenes to bind monovalent, divalent and trivalent cations has been widely reported [4,5]. The increasing interest in the interaction between lanthanides and calixarenes is due to their ability

to efficiently and selectively complex and extract those elements. To bind hard lanthanide cations, residues with hard oxygen donor atoms, such as phosphine oxides [6,7], carboxylic acids [8–10] or amides [8,11,12], have been introduced in the calixarene frameworks. Ketone moieties have also been incorporated in either the upper or the lower rims of these macrocycles [13,14].

We have been conducting a systematic study on the binding properties of dihomooxacalix[4]arenes (calix[4]arene analogues in which one CH$_2$ bridge is replaced by one CH$_2$OCH$_2$ group) [15] bearing carbonyl groups (ester [16,17], ketone [18,19] and amide [20,21]) at the lower rim towards several cations with different valences. Herein, we complete this study, presenting our results concerning the lanthanide ion binding by dihomooxa ketone ligands.

This article presents the binding properties of four tetraketone (methyl **1a** [22], *tert*-butyl **1b** [22], adamantyl **1c** [22,23] and phenyl **1d** [24]) derivatives of *p-tert*-butyldihomooxacalix[4]arene (Fig. 1) towards several lanthanide cations. These properties have been assessed by extraction studies of metal picrates from an aqueous solution into dichloromethane and stability constant measurements in acetonitrile based on UV absorption spectrophotometry. The affinity of the ligands for selected cations (La^{3+}, Eu^{3+}
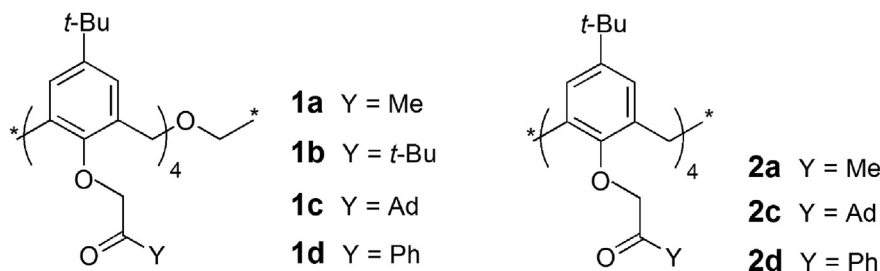

Fig. 1. Structural formulae of calixarenes.

and Yb^{3+}) has also been investigated by proton NMR experiments. Molecular dynamics (MD) and potential of mean force (PMF) simulations were performed in pure acetonitrile and dichloromethane solutions and at a dichloromethane/water interface to bring further structural and energetic insights into the binding and extraction processes. Tetraketone (methyl **2a**, adamantyl **2c** and phenyl **2d**) derivatives of *p-tert*-butylcalix[4]arene (Fig. 1) were also studied in the present work, and the results of all ligands were compared and discussed in terms of the substituent groups attached to the ketone function, as well as the size and conformational effects of the macrocycles.

2. Results and discussion

2.1. Extraction studies

The ionophoric properties of tetraketones **1a-d** and **2a**, **2c** and **2d** towards lanthanide metal cations were evaluated by the standard picrate extraction method [25]. The results, expressed as a percentage of cation extracted (% *E*), are reported in Table 1. All the ketones had already been synthesised and obtained in the cone conformation, except methyl ketone **1a** that was obtained in a partial cone conformation.

The results obtained show that ketones **1b-1d** are modest extractants, showing preference for the heavy lanthanides Gd^{3+} and Yb^{3+}. The three ketones present similar extraction trends, with the two former displaying relatively higher percentages than the latter. The presence of the *tert*-butyl and adamantyl groups in ligands **1b** and **1c**, respectively, more donating than the phenyl group (**1d**), leads to a higher basicity of the carbonyl oxygen in the former derivatives. Adamantyl ketone **1c** is a slightly better phase-transfer agent than *t*-butyl ketone **1b** (Gd^{3+} = 23 and 19.1% *E*; Yb^{3+} = 21 and 18% *E*, respectively). A similar behaviour had already been observed previously by us towards monovalent and divalent cations [18,19]. Methyl ketone **1a**, in a partial cone conformation, is a very weak extractant (% *E* ranges from 3.3 to 5.8), being unable to discriminate among the lanthanide ions studied.

Concerning tetraketones **2a**, **2c** and **2d**, they exhibit very low extractability too (% *E* ranges from 4.1 to 8.5), showing almost no discrimination for the ten lanthanide ions. The higher conformational flexibility of the dihomooxacalix[4]arene macrocycle compared to that of the calix[4]arene may allow for a more suitable arrangement of the ketone pendant arms around the lanthanide cations, which require high coordination numbers, and thus favours their extraction. With regards to other dihomooxa ligands, such as the analogue ethylamide derivative [24], these dihomooxa ketones show an opposite extraction profile.

2.2. UV-vis complexation studies

Complexation of five representative lanthanide ions (La^{3+}, Pr^{3+}, Eu^{3+}, Gd^{3+} and Yb^{3+}) by tetraketone ligands **1b**, **1d** and **2d** was studied in acetonitrile by UV-vis absorption spectrophotometry. The spectral changes of the ligands upon stepwise addition of the metal triflates in solution allow the determination of the nature and the stability of the complexes formed. The stability constants (as log β) of the 1:1 complexes are presented in Table 2.

Some kinetic effects were observed, *i.e.* the time needed to reach the equilibrium was important with ligands **1b** and **1d**, in particular for Pr^{3+} (20 min) and to a lesser extent for the other lanthanide cations (between 5 and 10 min). In these cases, the experimental protocol had to be adapted either by waiting the time needed to reach the equilibrium between each addition or by preparing the mixtures in separated vials.

Important spectral variations were obtained with all ligands, as shown, for example, in Fig. 2 for Pr^{3+} with **1b**. These ligands present high affinities for all the lanthanides studied, displaying stability constants for the ML (metal:-ligand) complexes that range from 4.6 to 6.2 log units. *t*-Bu ketone **1b** forms more stable species than Ph ketone **1d**, which is consistent with the donor property of the *tert*-butyl group. Ph ketone **1d** is, however, a more selective

Table 2
Stability constants (log β)[a] for 1:1 lanthanide complexes in acetonitrile (T = 25 °C; $I = 10^{-2}$ M, Et_4NClO_4).

Ligands	La^{3+}	Pr^{3+}	Eu^{3+}	Gd^{3+}	Yb^{3+}
1b	6.1 ± 0.6	5.9 ± 0.6	5.7 ± 0.3	6.0 ± 0.5	5.5 ± 0.5
1d	6.0 ± 0.1	5.6 ± 0.7	4.9 ± 0.4	4.6 ± 0.9	4.8 ± 0.3
2d	5.1 ± 0.2	n.d.	n.d.	5.0 ± 0.2	6.2 ± 0.2

n.d: not determined.
[a] Confidence interval corresponding to $\pm \sigma n_{-1}$, σn_{-1} being the standard deviation on the mean value of at least two experiments.

Table 1
Extraction percentage of lanthanide picrates into CH_2Cl_2 at 25 °C[a].

	La^{3+}	Ce^{3+}	Pr^{3+}	Nd^{3+}	Sm^{3+}	Eu^{3+}	Gd^{3+}	Dy^{3+}	Er^{3+}	Yb^{3+}
Ionic radius[b]/Å	1.03	1.01	0.99	0.98	0.96	0.95	0.94	0.91	0.89	0.87
1a	4.9	4.5	3.3	4.6	4.5	5.0	4.4	5.8	5.6	5.1
1b	6.8	6.4	7.3	8.4	12.3	8.6	19.1	7.0	11.6	18.0
1c[c]	9.3	7.7	6.0	8.9	14	7.4	23	7.9	12	21
1d	8.9	6.0	6.7	7.3	10.5	5.7	13.4	7.5	7.8	16.0
2a	5.3	5.2	5.2	6.2	5.6	4.9	4.5	5.1	5.9	5.3
2c	6.8	6.3	4.5	5.5	6.4	5.0	5.1	4.8	4.9	4.6
2d	5.3	5.6	4.1	6.6	8.2	8.5	5.2	5.6	7.1	8.1

[a] Values with uncertainties less than 5%.
[b] R.D. Shannon, C.T. Prewitt, Acta Cryst. B25 (1969) 925; B26 (1970) 1046; data quoted in I. Marcus, *Ion Properties*, Marcel Dekker, New York, 1997, pp. 46–47.
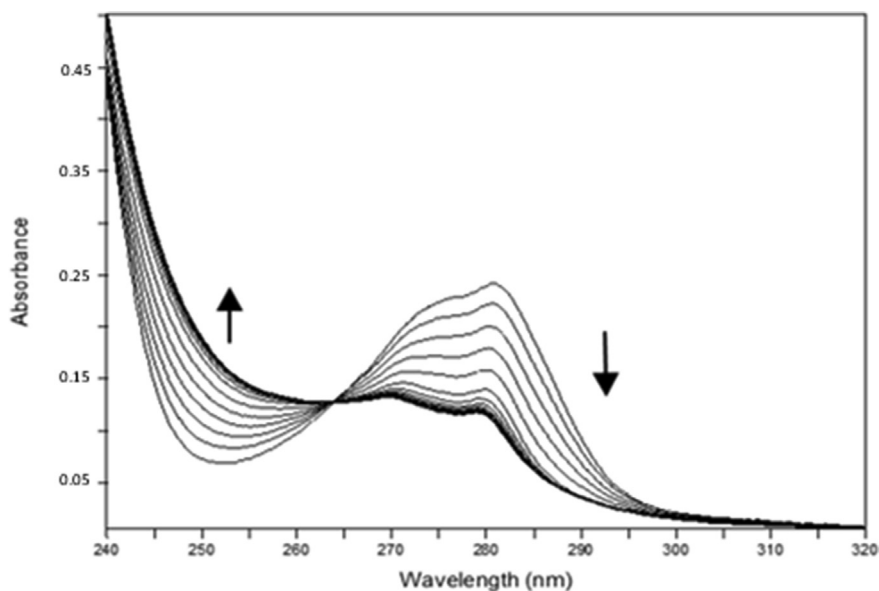[c] Data obtained from the study by Marcos et al. [23].

Fig. 2. Spectral variations corresponding to the complexation of Pr^{3+} with **1b** in acetonitrile at 25 °C ($C_L = 6.63 \times 10^{-5}$ M; $0 \le R = C_M/C_L \le 1.97$); $I = 10^{-2}$ M Et_4NClO_4.

ligand, showing a variation of almost 1.4 log units between the highest and the lowest log β values, in contrast to only 0.6 log units for ketone **1b**. Both dihomooxa ketones exhibit a similar behaviour, with preference for the light lanthanides (La^{3+} and Pr^{3+}). The studies with Ph ketone **2d** allowed us to determine the influence of the oxygen bridge and consequently of the size and the flexibility of the macrocycles on the cation complexation. The results with ligand **2d** showed a reverse behaviour in respect to its dihomooxa homologous, as **2d** displayed a preference for the heavy and smaller lanthanide Yb^{3+}.

The comparison with the analogue ethylamide [24] brings out that these dihomooxa ketones, although weaker binders, are more selective ligands, mainly Ph ketone **1d**.

2.3. Proton NMR binding studies

To obtain further information on the binding behaviour of ketones **1a-d** and **2a**, **2c** and **2d**, specifically concerning the binding sites, proton NMR titrations were performed in $CDCl_3/CD_3OD$ with these ligands and La^{3+}, Eu^{3+} and Yb^{3+} cations, representatives of the light, middle and heavy categories of the lanthanide series, respectively. Variable amounts of the salts were added to the ligands, and the proton spectra were recorded after each addition.

Two different situations were found after the addition of La triflate to the ligands. No complexation was observed in the cases of dihomooxa Me ketone **1a** and the three ketones **2a**, **2c** and **2d**, while with the other dihomooxa ketones **1b–d** titrations induced broadening and chemical shift variation in the peaks, as shown in Fig. 3 for the titration of Ad ketone **1c**. Although the broad proton signals prevent a quantitative analysis of the data, it was possible to record downfield shift variations between 0.13 and 0.28 ppm for the aromatic protons of **1c** after the addition

of 1 equiv of La triflate. These results indicate a slow exchange rate between the free and the complexed species on the NMR time scale at room temperature. After subsequent addition of the salt (up to 2–3 equiv), the peaks remain broad but unchanged. This behaviour seems to indicate a strong affinity of the ligands for La^{3+}.

All the tetraketones exhibited similar behaviour towards Eu^{3+}. Small chemical shift variations were observed upon the addition of an excess of salt (3 equiv), indicating weak complexation with this cation.

Concerning Yb^{3+} complexation, the titrations with all the ketones produced broad peaks that become sharp after the addition of an excess of the salt, as shown in Fig. 4 for t-Bu ketone **1b**. These results should indicate interaction with the cation, although no meaningful upfield or downfield shift variations of the peaks were observed, as expected from the binding of a paramagnetic metal ion, such as Yb^{3+} [26].

In general, the NMR results follow the same trend of those obtained before by UV spectrophotometric studies.

2.4. MD simulations

2.4.1. Solvation in pure acetonitrile and dichloromethane

Simulation studies were mainly focused on the comparison between dihomooxacalix[4]arene and calix[4] arene derivatives. Thus, the affinity of Ph ketones **1d** and **2d** for La^{3+} and Yb^{3+} cations was obtained through MD simulations. These cations, representative of the light and heavy lanthanides, were chosen because of the highest difference on their E % and log β values. Picrate and triflate counterions were added to neutralise the chemical systems and to reproduce the extraction and complexation experiments in dichloromethane and acetonitrile, respectively. Dichloromethane solutions mimic the final organic phase
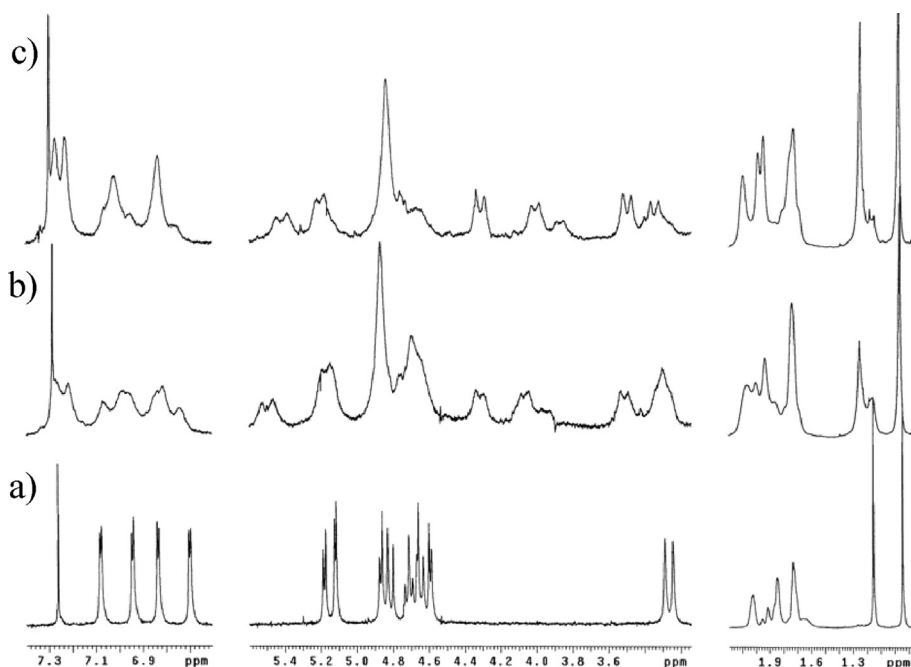
Fig. 3. 500 MHz ^{1}H NMR spectra of Ad ketone **1c** in CDCl$_3$ at 25 °C: (a) free ligand, (b) upon addition of 0.5 and (c) 1 equiv of La triflate.

once the extraction has taken place. Final structures obtained are given in Fig. 5, and interaction energies and radial distribution functions performed during the simulations are presented in Table 3 and in Fig. S1, respectively.

Simulations show some clear differences in the structures and solvation of the M^{3+}⊂**1d** and M^{3+}⊂**2d** complexes and significant interactions between the M^{3+} cations and the counterions.

The M^{3+}⊂**1d** complexes are asymmetrical owing to the presence of the supplementary oxygen atom, while **2d** leads to more symmetrical complexes with an equivalent participation of the oxygen atoms. The position of the La^{3+}
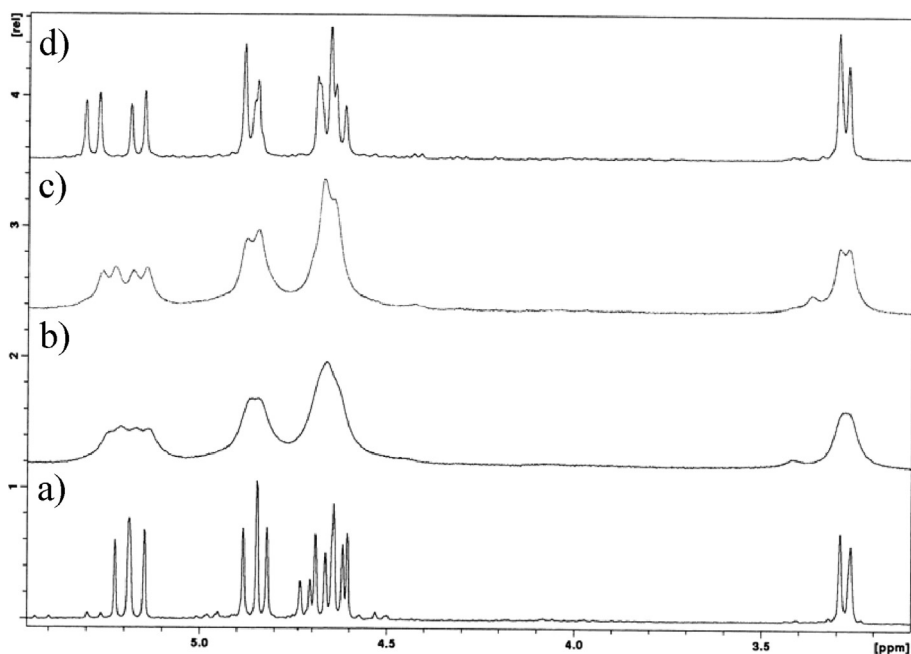

Fig. 4. Methylene region of the ^{1}H NMR spectra of *t*-Bu ketone **1b** in CDCl$_3$, 25 °C and 500 MHz: (a) free ligand, upon addition of (b) 0.5, (c) 1 equiv and (d) 3 equiv of Yb triflate.

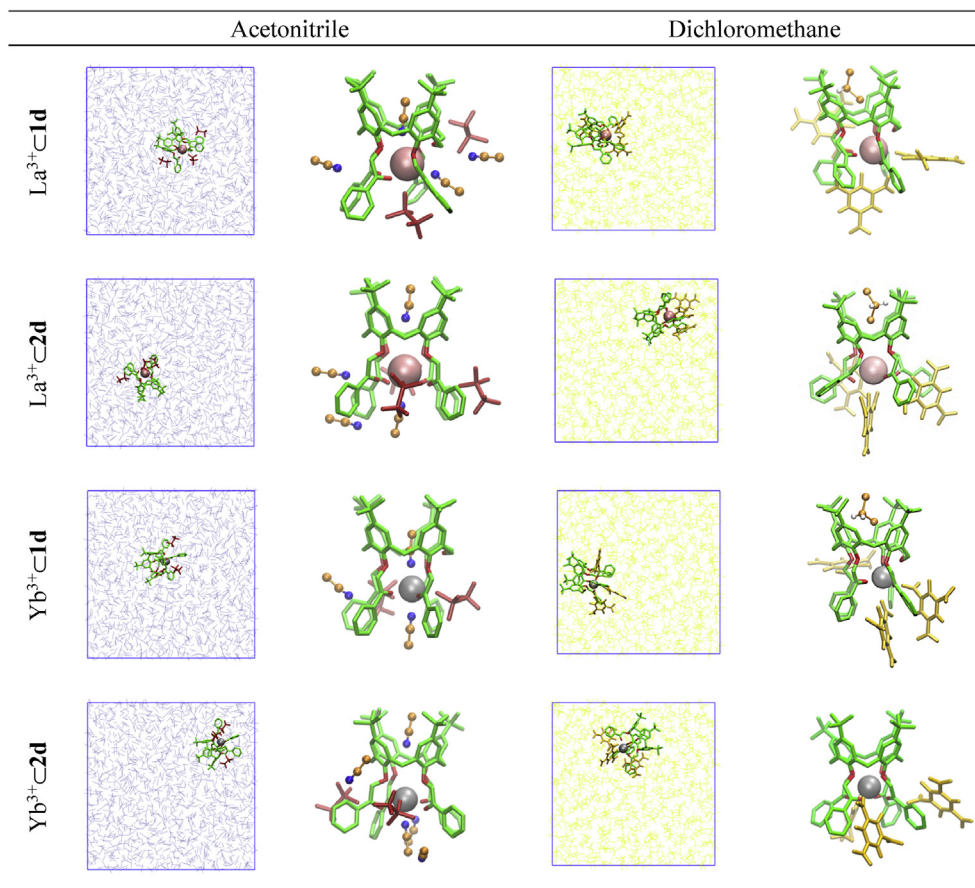**Fig. 5.** Final snapshots of $M^{3+} \subset$ **1d** and $M^{3+} \subset$ **2d** complexes in acetonitrile (left) and dichloromethane (right). Final views of the full simulation boxes and snapshots of the structures and solvation of the calixarenes.

cation within the cavity formed by the four phenoxy and the four carbonyl oxygen atoms of both ligands in aceto-nitrile and dichloromethane solvents is more centred when compared to that of Yb^{3+}. As clearly illustrated by the snapshots of Fig. 5, this smaller cation interacts with the ligands preferentially via the carbonyl oxygen atoms, which leads to a lower position in the cavity. However, in the case of $Yb^{3+} \subset$ **2d** in dichloromethane, the cation is perfectly centred in the cavity.

For both calixarenes, the coordination spheres of the lanthanide cations are completed by triflate anions and solvent molecules in acetonitrile (via the nitrogen atom of

the cyano groups) and picrate anions in dichloromethane. It is important to note that, on average, there are only two triflates around the complexes, which results in the for-mation of a $+1$ charged association. In dichloromethane solutions, three picrate anions sit into the first sphere of coordination of the lanthanide ions and interact with the $M^{3+} \subset$calixarene complexes, thus forming a neutral spe-cies. $M^{3+} \cdots$calixarene and $M^{3+} \cdots$anions radial distribution functions (RDFs; Fig. S1) calculated during the last 5 ns of dynamics clearly show the differences of interaction be-tween the ligands, the cations and the anions. The number of oxygen atoms around La^{3+} varies from 9.0 to 11.0 and

Table 3
Interaction energies (kcal mol^{-1}) in acetonitrile solution and gas phase.

	MD[a] acetonitrile solution						MD[a] vacuum	QM[b] vacuum
	M^{3+}	ligand	$M^{3+} \subset$ligand	$3X^-$	solute	solvent[c]		
$La^{3+} \subset$**1d**	−498		−544		−311		−534	−589.9
$La^{3+} \subset$**2d**	−508		−576		−240		−521	−581.9
$Yb^{3+} \subset$**1d**	−467		−813		−219		−649	−669.2
$Yb^{3+} \subset$**2d**	−577		−617		−229		−656	−672.4

[a] Calculated during the last 5 ns of dynamics; fluctuations are about 8 kcal mol^{-1}.
[b] QM B3LYP/6-31G(d,p) optimisations.
[c] Solute $= [M^{3+} \subset$ligand$\cdots 3X^-]$; $X^- =$ triflate anion.

around Yb^{3+} from 7.6 to 10.0. The first peak of the RDFs clearly show that the $O_{C=O} \cdots Yb^{3+}$ distances are always shorter than $O_{C=O} \cdots La^{3+}$ distances (2.4 vs 2.9), being consistent with the fact that La^{3+} has a higher radius than Yb^{3+}. This tendency is the same for the counterions. Moreover, for both cations, the picrate anions are always further away than the triflate anions. In all but one case, the upper rim of the calixarenes is filled with a solvent molecule (Fig. 5). This trapped molecule interacts with the complexed cation via an $N_{cyano} \cdots M^{3+}$ or $Cl \cdots M^{3+}$ interaction.

The interaction energies between the lanthanide cations and the two ligands in gas phase and in solution were calculated, and the results are reported in Table 3. Cation$\cdots$ligand interaction energies calculated in vacuum by quantum mechanics (QM) and MD simulations are

consistent and follow the same order. These energies are higher for the Yb^{3+} cation than for La^{3+} in agreement with the shorter $O_{C=O} \cdots M^{3+}$ distances observed before. For the majority of the cases studied, these values follow the same trend of the stability constants. In solution, the cation$\cdots$ligand energies are lower; the variations are quite low for the La^{3+} cation (from 13 to 36 kcal mol^{-1}) and much higher for Yb^{3+} (from 79 to 182 kcal mol^{-1}). These differences are compensated by a better interaction between the $Yb^{3+} \subset$ ligand and the triflate anions.

2.4.2. Free energy calculations at the dichloromethane/water interface

To get further insights of the extraction process, PMF calculations were performed at the dichloromethane/water interface. The free energy profiles were calculated for
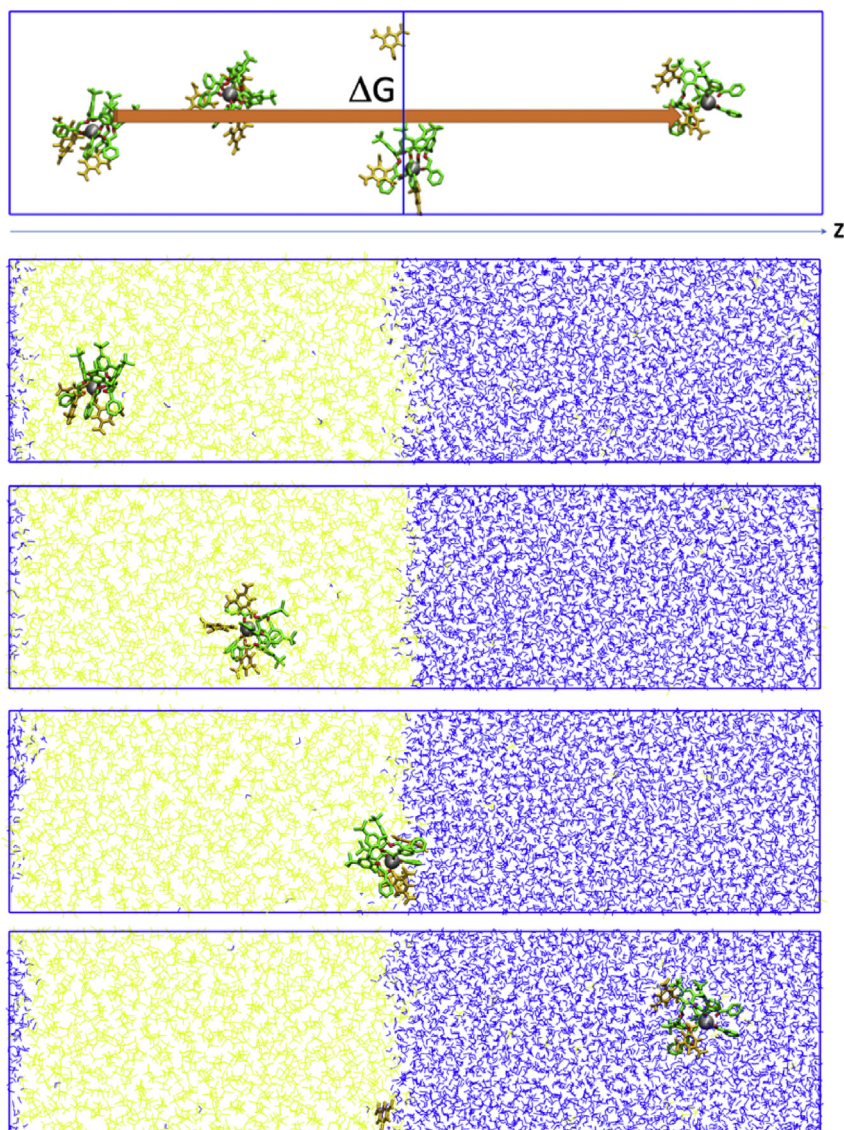

Fig. 6. $Yb^{3+} \subset \mathbf{2d} \cdots 3Pic^-$ system at a CH_2Cl_2/water interface (CH_2Cl_2 represented in yellow and water in blue). Scheme of the procedure of the PMF calculations (top) and different snapshots during the dynamics of interface crossing (bottom). A precise description of the PMF calculation can be found in the Supporting Information.
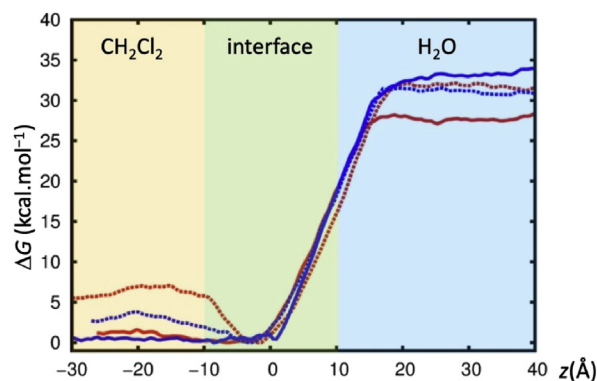
Fig. 7. PMF calculations crossing the CH$_2$Cl$_2$/H$_2$O interface with picrate anions. Free energies ΔG (kcal mol^{-1}) as a function of the distance Z (Å). In red: La^{3+}⊂**1d** (full), La^{3+}⊂**2d** (dotted); in blue: Yb^{3+}⊂**1d** (full), Yb^{3+}⊂**2d** (dotted).

M^{3+}⊂calixarene interface crossing for both **1d** and **2d** with picrate as a counter ion. Free energies were calculated as a function of the z-position of the complex (Fig. 6). The initial positions of the calixarenes were obtained after 10 ns of MD runs at the dichloromethane/water interface. The complexed calixarenes sit into the organic phase or at the interface between the two liquids (Fig. 6).

Calculated free energy profiles are reported in Fig. 7; although these values are unknown, it is clear from extraction experiments that the lanthanide cations are extracted and thus prefer the organic phase. The transfer to the organic phase is found to be very similar for La^{3+} and Yb^{3+} cations and is almost independent of the nature of the calixarene used which is consistent with the moderate extraction rate of ligands **1d** and **2d**. To retain the neutrality of the source and receiving phases, the cation's charge is compensated by counterions to be extracted. Free energy of transfer shows a clear energetic preference of both M^{3+}⊂calixarene for dichloromethane, as well as small differences in the extraction of La^{3+} and Yb^{3+} by **1d** and **2d**. PMF curves nicely follow the extraction percentages measured experimentally: The free energy calculated for Yb^{3+}⊂**1d** (full blue curve, Fig. 7) shows no minima at the interface and a large energy gap between water and the organic phase, which indicates that the extraction process is spontaneous. The same conclusion applies to La^{3+}⊂**1d**, with an energy gap a little bit smaller (full red curve, Fig. 7). The two curves for ligand **2d** show a small energy minimum of about 3–6 kcal mol^{-1} at the interface. This indicates that the M^{3+}⊂**2d** species should be trapped and accumulates at the interface, being the diffusion to dichloromethane harder. This observation can also explain the smaller extraction percentages obtained for this ligand compared to those of **1d**.

3. Conclusions

Extraction studies from an aqueous solution into CH$_2$Cl$_2$ have indicated that dihomooxa ketones **1b**–**1d**, in the cone conformation, are modest extractants for the lanthanides, displaying some preference for Gd^{3+} and Yb^{3+} cations (% E = 23 and 21, respectively, for **1c**). In the case of classical

calix[4]arenes, ketones **2a**, **2c**, and **2d** presented low percentages of extraction (% E ≤ 8.5), with almost no discrimination among the ten lanthanides studied. The stability constants obtained in acetonitrile have shown however that both types of ligands are good binders, with some selectivity for La^{3+} in the case of ketones **1b** and **1d** (log β = 6.1 and 6.0, respectively) and for Yb^{3+} in the case of **2d** (log β = 6.2). NMR titration results indicated a similar binding trend as that observed by UV studies. Phenyl ketone **1d** showed to be a slightly weaker ligand than *tert*-butyl **1b** and adamantyl **1c**, being in agreement with the basicity of their carbonyl oxygen atoms.

MD and PMF simulations performed for ligands **1d** and **2d** with La^{3+} and Yb^{3+} cations in acetonitrile and dichloromethane, and at a CH$_2$Cl$_2$/water interface, were consistent with the experimental results. The calculations showed features of each ligand (**1d** vs **2d**) and the role of counterions in the complexation. Calculated free energy profiles for M^{3+}⊂calixarene interface crossing demonstrated that its transfer to the organic phase is energetically favourable. Overall, simulations provided explanations, at the microscopic level, that contribute to a better understanding of the differences between ligands **1d** and **2d** observed experimentally.

4. Experimental

4.1. Extraction studies

After mutual saturation of the solvents, equal volumes (5 mL) of aqueous solutions of metal picrates (2.5×10^{-4} M) and solutions of the calixarenes (2.5×10^{-4} M) in CH$_2$Cl$_2$ were vigorously shaken for 2 min and then thermostated in a water bath with mechanical stirring at 25 °C overnight. After complete phase separation, the absorbance A of picrate ions in the aqueous phase was determined spectrophotometrically (λ_{max} = 354 nm). For each cation-calixarene system the absorbance measurements were repeated at least four times. Blank experiments without calixarene were run under the same conditions, yielding an absorbance A_0. The percentage of cation extracted was calculated as the ratio $100 \times (A_0 - A)/A_0$. The details of the metal picrate preparation have already been described [23].

4.2. Determination of stability constants

The apparent overall stability constants β, defined as the concentration ratio [ML^{n+}]/([M^{n+}][L]) (where M^{n+} = cation and L = ligand), were determined in acetonitrile (Chromasolv@gradient grade for HPLC ≥99.9%, used without further purification; Sigma-Aldrich) by absorption spectrophotometry. The spectra were recorded between 240 and 350 nm using a Shimadzu UV-2401 PC spectrophotometer using quartz cells (Hellma) with an optical path length of 1 cm. Successive additions of the metal salt solution were made to 2.5 mL of a ligand solution (C_L = 1.8×10^{-5} – 8.5×10^{-5} M) directly in the spectrophotometric cell. When kinetic effects were observed, solutions were prepared in separated vials and measured after the time needed to reach the equilibrium. The experiments were performed at 25 °C and constant ionic strength provided by

10^{-2} M Et$_4$NClO$_4$ (98%; Acros Organics). The spectral changes were interpreted using the numerical program SpecFit [27]. The metal salts used were triflates: La(CF$_3$SO$_3$)$_3$,2.7H$_2$O (99%; Alfa Aesar); Pr(CF$_3$SO$_3$)$_3$,3.6H$_2$O(98%; Alfa Aesar); Eu(CF$_3$SO$_3$)$_3$,3.2H$_2$O (98%; Alfa Aesar); Gd(CF$_3$SO$_3$)$_3$,13H$_2$O (98%; Alfa Aesar); Yb(CF$_3$SO$_3$)$_3$,1.4H$_2$O (99.99%; Sigma-Aldrich). All these salts were dried under vacuum for at least 24 h before use. The concentrations of their stock solutions were standardised by complexometry titrations with ethylenediaminetetraacetic acid using the xylenol orange as a coloured indicator [28].

4.3. Proton NMR titrations

Several aliquots (up to 3 equiv) of the salt solutions in CD$_3$OD were added to CDCl$_3$ solutions (5×10^{-3} M) of the ligands directly in the NMR tube. The salts used were La, Eu and Yb triflates. Owing to the low solubility of Eu triflate in MeOH, it was necessary to decrease the concentration of the ligands (2.5×10^{-4} M) and of the salt accordingly. The spectra were recorded on a Bruker Avance III 500 Spectrometer after each addition of the salts. The temperature of the NMR probe was kept constant at 25 °C.

4.4. MD simulations

The solutions have been simulated by classical MD simulations using the Amber18 software [29], in which the potential energy U is empirically represented by a sum of bond and angle harmonic deformations, of dihedral torsions, and by pairwise additive 1-6-12 (electrostatic + van der Waals) interactions between nonbonded atoms (Eq. 1):

$$U = \sum_{\text{bonds}} k_r (r - r_0)^2 + \sum_{\text{angles}} k_\theta (\theta - \theta_0)^2$$
$$+ \sum_{\text{dihedrals}} k_\phi [1 + \cos(n\phi + \phi_0)]$$
$$+ \sum_{\text{atom } i} \sum_{j \neq i} 4\varepsilon_{i,j} \left[\left(\frac{\sigma_{i,j}}{r_{i,j}}\right)^{12} - \left(\frac{\sigma_{i,j}}{r_{i,j}}\right)^6 \right] + \sum_{\text{atom } i} \sum_{j \neq i} \frac{q_i q_j}{\varepsilon_0 r_{i,j}} \quad (1)$$

A full description of the simulation parameters, PMF procedure and analysis is given in the Supporting Information.

Acknowledgements

Appendix A. Supplementary data

Supplementary data to this article can be found online at https://doi.org/10.1016/j.crci.2019.09.005.

References

[1] F. Arnaud-Neu, Radiochim. Acta 91 (2003) 659–664.
[2] S. Faulkner, S.J.A. Pope, B.P. Burton-Pye, Appl. Spectrosc. Rev. 40 (2005) 1–31.
[3] J.-C.G. Bünzli, Acc. Chem. Res. 39 (2006) 53–61.
[4] F. Arnaud-Neu, M.A. McKervey, M.J. Schwing-Weill, in: Z. Asfari, V. Böhmer, J. Harrowfield, J. Vicens (Eds.), Calixarenes 2001, Kluwer Academic Publishers, Dordrecht, 2001, pp. 385–406.
[5] B.S. Creaven, D.F. Donlon, J. McGinley, Coord. Chem. Rev. 253 (2009) 893–962.
[6] M. Karavan, F. Arnaud-Neu, V. Hubscher-Bruder, I. Smirnov, V. Kalchenko, J. Incl. Phenom. Macrocycl. Chem. 66 (2010) 113–123.
[7] S.R. Menon, J.A.R. Schmidt, Tetrahedron 72 (2016) 767–774.
[8] P.D. Beer, G.D. Brindley, O.D. Fox, A. Grieve, M.I. Ogden, F. Szemes, M.G.B. Drew, J. Chem. Soc., Dalton Trans. (2002) 3101–3111.
[9] A.B. Chetry, T. Matsufuji, B.B. Adhikari, S. Morisada, H. Kawakita, K. Ohto, T. Oshima, Jumina, J. Incl. Phenom. Macrocycl. Chem. 81 (2015) 301–310.
[10] X. Lu, D. Zhang, S. He, J. Feng, A.T. Reda, C. Liu, Z. Yang, L. Shi, J. Li, Sep. Purif. Technol. 188 (2017) 250–259.
[11] A. Casnati, N. Della Ca, M. Fontanella, F. Sansone, F. Ugozzoli, R. Ungaro, K. Liger, J.-F. Dozol, Eur. J. Org. Chem. (2005) 2338–2348.
[12] F. Glasneck, K. Kobalz, B. Kersting, Eur. J. Inorg. Chem. (2016) 3111–3122.
[13] R. Zairov, N. Shamsutdinova, S. Podyachev, S. Sudakova, G. Gimazetdinova, I. Rizvanov, V. Syakaev, V. Babaev, R. Amirov, A. Mustafina, Tetrahedron 72 (2016) 2447–2455.
[14] S. Podyachev, G. Gimazetdinova, S. Sudakova, N. Shamsutdinova, D.V. Lapaev, V. Syakaev, A.T. Gubaidullin, R.N. Nagimov, A.R. Mustafina, Tetrahedron 73 (2017) 5397–5407.
[15] P.M. Marcos, in: P. Neri, J.L. Sessler, M.-X. Wang (Eds.), Calixarenes and beyond, Springer International Publishing Switzerland, 2016, pp. 445–466.
[16] P.M. Marcos, J.R. Ascenso, M.A.P. Segurado, J.L.C. Pereira, Tetrahedron 57 (2001) 6977–6984.
[17] P.M. Marcos, J.R. Ascenso, M.A.P. Segurado, J.L.C. Pereira, J. Incl. Phenom. Macrocycl. Chem. 42 (2002) 281–288.
[18] P.M. Marcos, S. Félix, J.R. Ascenso, M.A.P. Segurado, B. Mellah, R. Abidi, V. Hubscher-Bruder, F. Arnaud-Neu, Supramol. Chem. 18 (2006) 285–297.
[19] P.M. Marcos, S. Félix, J.R. Ascenso, M.A.P. Segurado, P. Thuéry, B. Mellah, S. Michel, V. Hubscher-Bruder, F. Arnaud-Neu, New J. Chem. 31 (2007) 2111–2119.
[20] P.M. Marcos, S. Félix, J.R. Ascenso, M.A.P. Segurado, J.L.C. Pereira, P. Khazaeli-Parsa, V. Hubscher-Bruder, F. Arnaud-Neu, New J. Chem. 28 (2004) 748–755.
[21] P.M. Marcos, J.R. Ascenso, M.A.P. Segurado, P.J. Cragg, S. Michel, V. Hubscher-Bruder, F. Arnaud-Neu, Supramol. Chem. 23 (2011) 93–101.
[22] S. Félix, J.R. Ascenso, R. Lamartine, J.L.C. Pereira, Tetrahedron 55 (1999) 8539–8546.
[23] P.M. Marcos, J.R. Ascenso, M.A.P. Segurado, R.J. Bernardino, P.J. Cragg, Tetrahedron 65 (2009) 496–503.
[24] P.M. Marcos, J.R. Ascenso, M.A.P. Segurado, J.L.C. Pereira, J. Phys. Org. Chem. 12 (1999) 695–702.
[25] C. Pedersen, J. Am. Chem. Soc. 92 (1970) 391–394.
[26] B. Lambert, V. Jacques, J.F. Desreux, in: G.J. Lumetta, R.D. Rogers, A.S. Gopalan (Eds.), Calixarenes for Separations. ACS Symposium Series 757, American Chemical Society, Washington, 2000, pp. 165–178.
[27] H. Gampp, M. Maeder, C.J. Meyer, A.D. Zuberbuehler, Talanta 32 (1985) 257–264.
[28] E. Merck, Méthodes d'analyses complexométriques par les Titriplex, 3ème ed., Grafis, Darmstadt, 1992.
[29] D.A. Case, I.Y. Ben-Shalom, S.R. Brozell, D.S. Cerutti, T.E. Cheatham III, V.W.D. Cruzeiro, T.A. Darden, R.E. Duke, D. Ghoreishi, M.K. Gilson, H. Gohlke, A.W. Goetz, D. Greene, R. Harris, N. Homeyer, S. Izadi, A. Kovalenko, T. Kurtzman, T.S. Lee, S. LeGrand, P. Li, C. Lin, J. Liu, T. Luchko, R. Luo, D.J. Mermelstein, K.M. Merz, Y. Miao, G. Monard, C. Nguyen, H. Nguyen, I. Omelyan, A. Onufriev, F. Pan, R. Qi, D.R. Roe, A. Roitberg, C. Sagui, S. Schott-Verdugo, J. Shen, C.L. Simmerling, J. Smith, R. Salomon-Ferrer, J. Swails, R.C. Walker, J. Wang, H. Wei, R.M. Wolf, X. Wu, L. Xiao, D.M. York, P.A. Kollman, AMBER 2018, University of California, San Francisco, 2018.